Development and Calibration of a Real-Time Airborne Radioactivity Monitor Using Gamma-Ray Spectrometry on a Particulate Filter

R. Casanovas, J. J. Morant, and M. Salvadó

***Abstract*—In this work, we present the development and calibration of a Real-time Airborne Radioactivity Monitor using gamma-ray spectrometry on a particulate Filter (RARM-F) to be used in an automatic environmental radiation surveillance network. The RARM-F collects a constant flow of air that passes across a particulate filter, where airborne aerosols are collected. Then, the filter is faced toward a NaI(Tl) or $\mathrm{LaBr_3(Ce)}$ scintillation detector that is used for gamma-ray spectrometry. This permits the identification and quantification of airborne radioactive isotopes in real time. The RARM-F was fully calibrated with a combination of experimental data and Monte Carlo simulations. For the simulations, a user code, including a model of the system geometry, was prepared for the EGS5 code system and validated with experimental measurements. The calibration methodology is independent of the scintillation crystal used; however, the measurement capabilities and the performance of the RARM-F are not. Thus, we also discuss some characteristics of the RARM-F when using different crystals.**

***Index Terms*—Calibration, environmental radiation monitoring, gamma-ray scintillation detectors, Monte Carlo methods, spectroscopy, surveillance.**

I. Introduction

THE main objective of an automatic real-time environmental radiation surveillance network is to detect anomalous levels of radioactivity in the environment as quickly as possible. The Spanish automatic network is essentially composed of two types of monitors [1]: aerosol and Geiger monitors. On the one hand, the aerosol monitors give artificial alpha and beta, radon and gamma (due mainly to the iodine isotopes) activity concentrations. On the other hand, the Geiger monitors give the ambient dose equivalent rate.

However, the obtained radiological values in the aerosol monitors cannot easily be interpreted in terms of the Spanish legislation because the legal limits established for the concentrations of activity are only set for individual isotopes. Therefore, the implementation of automatic in-situ gamma-ray spectrometry was identified as a possible solution in a previous study [1]. When gamma-ray spectrometry is used instead of gross counting, it is possible not only to identify the involved isotopes in a radiation level increment but also to quantify their activity concentrations. Hence, this enables the discrimination of naturally occurring radionuclides from artificial ones and the establishment of automatic alerts based on the limits provided by legislation.

The use of automatic in-situ gamma-ray spectrometry is fairly common in radiation surveillance networks. Two examples of this are the International Monitoring System (IMS) of the Comprehensive Test Ban Treaty Organization with the Radionuclide Aerosol Sampler/Analyzer (RASA) [2] and the $\mathrm{LaBr_3(Ce)}$ nationwide radiation monitoring network of Finland [3].

On the one hand, the RASA is an automated high volume ($500\ \mathrm{m^3/h}$) aerosol collector equipped with a high-purity germanium (HPGe) detector that provides high-resolution gamma-ray spectrometry. The overall duration of a measurement cycle is 72 h, and thus, it cannot be used as an early warning system. Concerning this, an upgrade including a NaI/CsI detector inside the sample head has been recently proposed [4].

On the other hand, the Finnish nationwide radiation monitoring network is composed of $\mathrm{LaBr_3(Ce)}$ detectors measuring directly the environmental radioactivity. The spectra are collected and analyzed every 10 minutes, and thus, the data can be used for early warning.

To develop an early warning system with better measurement capabilities than those obtained by direct measurement, a Real-time Airborne Radioactivity Monitor using gamma-ray spectrometry on a particulate Filter (RARM-F) was developed by Universitat Rovira i Virgili, Universitat Politècnica de Catalunya and Raditel Serveis i Subministraments Tecnològics S.L. The RARM-F is basically composed of an aerosol collector and a scintillation detector, either a NaI(Tl) or a $\mathrm{LaBr_3(Ce)}$ detector.

The use of scintillators, instead of HPGe detectors, avoids failures related to the mechanical coolers, which have been identified as a significant portion of missing data in RASA [4]. In this paper, we describe the general aspects of the RARM-F development, as well as its full calibration procedure, which is performed by combining experimental measurements with Monte Carlo (MC) simulations.

Manuscript received June 28, 2012; revised October 24, 2012; accepted January 06, 2014. Date of publication February 21, 2014; date of current version April 10, 2014.

R. Casanovas and M. Salvadó are with the Unitat de Física Mèdica, Falcultat de Medicina i Ciències de la Salut, Universitat Rovira i Virgili, ES-43201 Reus (Tarragona), Spain (e-mail: ramon.casanovas@urv.cat).

J. J. Morant is with the Servei de Protecció Radiològica, Servei de Recursos Científics i Tècnics, Universitat Rovira i Virgili, ES-43007 Tarragona, Spain.

Color versions of one or more of the figures in this paper are available online at http://ieeexplore.ieee.org.

Digital Object Identifier 10.1109/TNS.2014.2299715

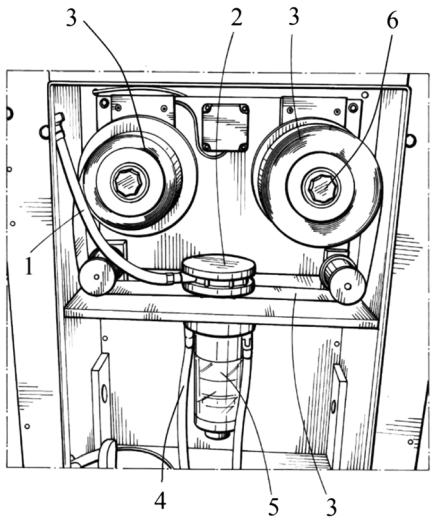

Fig. 1. Front view scheme of the RARM-F without Pb shielding. The main elements are: inlet duct (1), head collector (2), fiber glass filter (3), outlet duct (4), scintillation detector (5) and motorized roller (6).

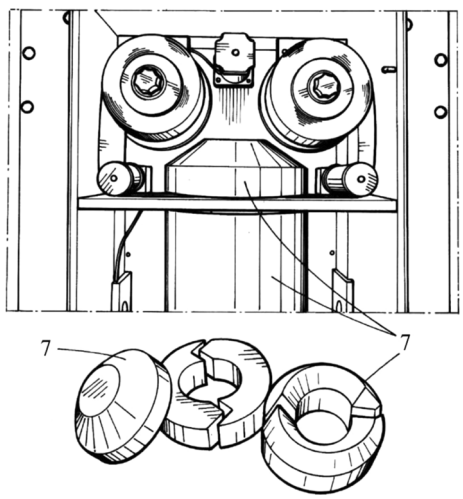

Fig. 2. Front view scheme of the RARM-F with the Pb shielding (7).

II. Materials

A. Description of the RARM-F

A general scheme of the developed monitor [5] is shown in Fig. 1 and Fig. 2. The system comprises a suction pump that collects a constant flow of air that can be preset by the user. The air is circulated through an inlet duct (1) towards a head collector (2). The head collector homogenizes and distributes the air flux in a circle 45 mm in diameter that passes across the particulate filter (3). The filter is used to retain the airborne particles and to accumulate the radioactive isotopes. Once the air has passed through the filter, it is expelled via an outlet duct (4).

The active part of the filter is faced toward a 2" x 2" NaI(Tl) or $LaBr_3(Ce)$ detector (5) connected to a multichannel analyzer, which permits the measurement of the gamma particle energy spectrum. After the selected integration time, the head collector is elevated and the filter is displaced with a motorized roller (6) to obtain the next set of measurements on a clean sheet of filter.

Both the detector and the active part of the filter are inside a cylindrical Pb shielding (7) 50 mm thick, which is used to reduce the surrounding background radiation and to avoid cross-contamination from the sheet of filter that is not being measured.

The NaI(Tl) detector was Model 905-3 from ORTEC and the $LaBr_3(Ce)$ detector was BrilLanCe380 from Saint-Gobain Crystals. The Pb shielding was specifically designed for this monitor and was manufactured by TECNIBUSA Protección Radiológica S.L.

The RARM-F has multiple control sensors (crystal temperature, air temperature, temperature in the rack, air flow, amount of filter available, positioning and traveling distance of the filter, filter break sensor, etc.). Software was specifically designed for local or remote control to manage data collection and storage, information transmission, sensor management, information on operating parameters, graphical representations of spectra, calculations, etc. The system also includes a meteorological station for observing atmospheric conditions. In addition, the RARM-F can easily integrate several devices, such as Geiger detectors or proportional counters, to complement the radiological measurements.

The obtained data are transmitted to a main server via an ADSL connection (using the SSL/TLS protocol), and remote control of the system is carried out using the TCP/IP protocol. However, other redundant means of communications are possible (GSM, radiofrequency, satellite, etc.). From the main server, it is also possible to activate alternative measurement systems (e.g. high flow filters for laboratory analysis) and to send automatic messages (SMS or emails) to a predefined contact list in response to either radiological criteria or different sensor signals.

Two prototypes of the RARM-F were constructed, one with a NaI(Tl) detector and the other with a $LaBr_3(Ce)$ detector, and have been continuously working in test phase since late 2009 and late 2010, respectively. Both monitors are housed inside a modular building, which permits a better control of their environmental conditions, but they take the air from outside. The modular building is located in the vicinity of a nuclear power plant.

B. Radioactive Calibration Sources

The experimental data were obtained from five certified radioactive point-sources that spanned the range of gamma energies up to 1408 keV. The available sources were ^{241}Am, ^{133}Ba, ^{137}Cs, ^{60}Co and ^{152}Eu. However, to reproduce the real counting geometry of the RARM-F, two calibration filters containing ^{241}Am and ^{137}Cs were prepared in the laboratory with an active diameter of 45 mm and a total activity of 20 Bq. To prepare each calibration filter, 2 mL of a certified liquid sample were uniformly distributed over the active part of the filter and dried at 45°C.

III. Methods

A. Experimental Setup

Calibration Methodology: The calibration methodology for NaI(Tl) and $\mathrm{LaBr_3(Ce)}$ detectors has been described in detail in a previous paper [6] and was adapted specifically for this monitor. This methodology encompasses the energy, resolution and efficiency calibrations. The experimental efficiencies were calculated from the $^{241}\mathrm{Am}$ and $^{137}\mathrm{Cs}$ calibration filters, which were prepared in the laboratory. These isotopes have simple decay schemes, emitting monoenergetic gamma rays, and therefore true coincidence summing is avoided.

The spectra stabilization against temperature changes is performed by means of software algorithms [7]. Besides, some digital systems with automatic gain correction have been tested for future upgrades.

Minimum Detectable Activity Concentration (MDAC): After calibration, the detection capabilities can be evaluated with the Minimum Detectable Activity Concentration (MDAC). The MDAC was determined using the following adaptation of the Currie expression [8] (for a detection limit with a 95% confidence limit):

$$MDAC = \frac{2.71 + 4.65\sqrt{B}}{\varepsilon \cdot V \cdot t \cdot p_\gamma} \tag{1}$$

where B is the number of background counts produced in a certain region of the spectrum (set symmetrically to the considered gamma ray), ε is the efficiency, V the aspired air volume, t the counting time and p_γ is the emission probability of the particular gamma ray being considered.

The radiation background is dominated by the ambient radon and thoron concentration, which is not constant along the day. To account this, we studied the real background of the monitors at different moments to provide a range of values of the MDACs. Thus, we calculated the minimum and maximum MDACs, in different integration times, corresponding with the minimum and maximum radon concentrations measured by the monitors.

B. Monte Carlo Simulations

The MC simulations were performed with the EGS5 code system [9]. This general-purpose package enables the simulation of the coupled transport of electrons and photons in an arbitrary geometry. For the control of the EGS5 subroutines, a previously validated user code [6] was adapted to the particularities of the RARM-F counting geometry.

A model of the RARM-F (see Fig. 3) was implemented by accounting for the real shapes, dimensions and materials of the elements involved in the radiation detection. Thus, the $\mathrm{NaI/LaBr_3}$ detectors were modeled with the corresponding scintillation crystal (green) in a case of aluminum 0.5 mm thick (red). The space between the case and the crystal was filled with air. A glass light guide behind the crystal (orange) was also considered, and the photomultiplier tube was modeled as a filled-of-air cylinder of aluminum (red). All of these elements were included inside a 50 mm Pb shield (blue), and the aluminum plate holding the filter was also modeled (red). The information on the materials (density and composition) was taken from [10], and the cut-off energy for the photons and the electrons was set at 10 keV.

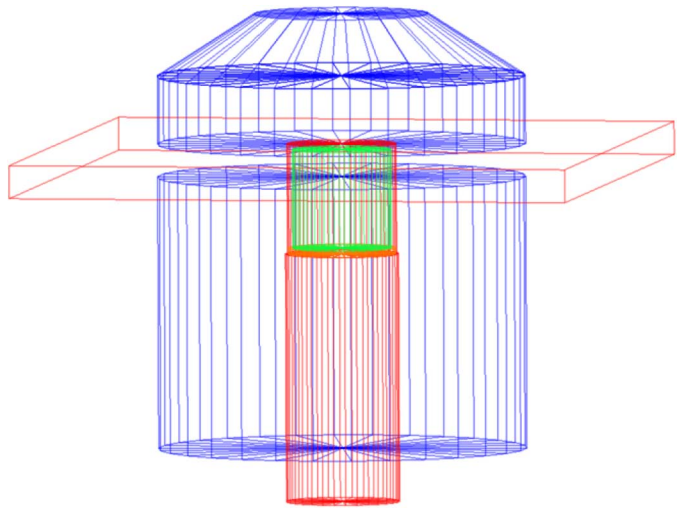

Fig. 3. Model of the RARM-F geometry (in scale) used in the MC simulations. The corresponding elements are NaI(Tl) or $\mathrm{LaBr_3(Ce)}$ crystal (green), light guide (orange), crystal case of Al (red), aluminum plate holding the filter (red) and Pb shield (blue).

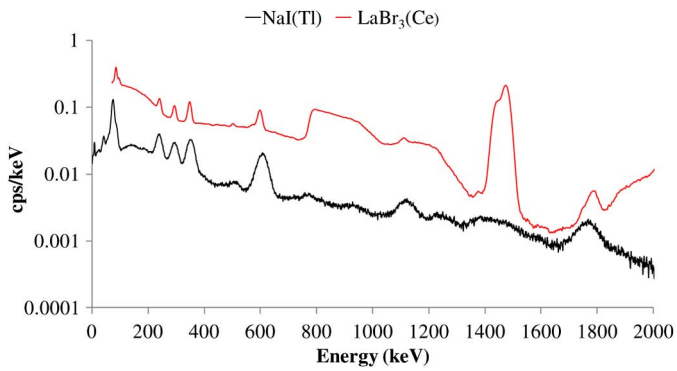

Fig. 4. Comparison of the typical background spectra obtained with both detectors in a 24 hour integration.

For the MC efficiency calculations, each point of the efficiency curve was calculated considering a monoenergetic source (in the range of 20 to 2000 keV) emitting in all directions with equal probability. The source was distributed homogeneously in a 45 mm diameter circle emulating the active part of the paper filter, which corresponds to the real counting geometry.

The MC efficiency ε_{MC} was calculated as:

$$\varepsilon_{MC} = \frac{N_{counts}}{N_{hist}} \tag{2}$$

where N_{counts} is the number of counts under the full energy peak and N_{hist} is the number of simulated histories (i.e., the number of primary source-particles simulated and all of the secondary particles produced by it), which was set to $2 \cdot 10^7$.

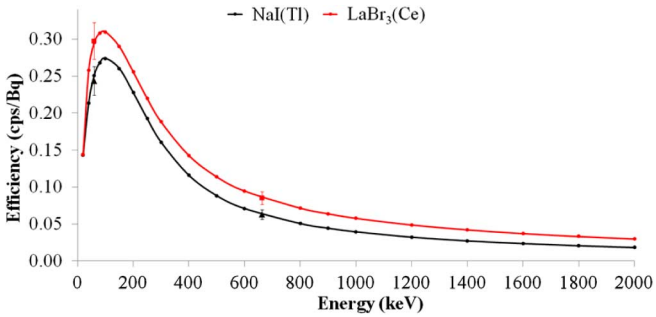

Fig. 5. Efficiency curves for the NaI(Tl) and the $LaBr_3(Ce)$ detectors. The experimental efficiencies are also shown (black triangles and red squares, respectively).

IV. Results and Discussion

A. Comparison of the Obtained Spectra

To show the performance of the RARM-F when using either the NaI(Tl) detector or the $LaBr_3(Ce)$ detector, two 24 hour integration spectra of the typical background are compared in Fig. 4.

The background spectra depicted clearly the peaks caused by radon daughters. In particular, the contributions of ^{214}Pb (239, 295 and 352 keV) and ^{214}Bi (609, 1120 and 1764 keV) could be observed. The peaks produced by these background isotopes can be overlapped with other from certain isotopes of interest, making it difficult to detect low amounts of them. In this sense, the better resolution observed in the $LaBr_3(Ce)$ detector makes it better at resolving close peaks of most of the isotopes of interest in environmental radiation monitoring.

An important difference observed in Fig. 4 was the background shape of the $LaBr_3(Ce)$ detector compared with the NaI(Tl) detector. Specifically, important differences can be clearly observed at approximately 789 keV and 1436 keV, which are the energies of the gamma particles emitted by the internal contamination of the ^{138}La in the $LaBr_3(Ce)$ crystal. Due to this contaminant, a beta continuum is also observed between these energies. As this self-background is practically constant (the half-life of the ^{138}La is $1.05 \cdot 10^{11}$ years), it could be removed from all the spectra after some analysis.

B. Efficiency Calculations

The efficiency curves implemented in the NaI(Tl) and the $LaBr_3(Ce)$ monitors are shown in Fig. 5. The efficiencies calculated with the MC simulations were multiplied by 0.85 and 0.90, respectively, to fit the experimental efficiencies (black triangles and red squares, respectively). In general, the MC values were higher than the experimental ones. These differences could be attributed to some simplifications introduced in the RARM-F model used in the simulations. For example, the filter is not modeled, although it produces some attenuation to the gamma rays. However, rather than complicating the geometry model, these differences can be overcome using a simple multiplication factor. Even so, more experimental values with other radionuclides at other energies should be obtained to check the validity of this approach at more points.

TABLE I
Comparison of the ^{137}Cs MDACs for Both Detectors Across Different Integration Times

	NaI(Tl) MDAC (Bq/m^3)		$LaBr_3$(Ce) MDAC (Bq/m^3)	
	min	max	min	max
10 min	3.8 (4)	8.3 (9)	2.1 (2)	2.3 (2)
1 h	0.25 (3)	0.57 (6)	0.14 (1)	0.15 (2)
12 h	0.0070 (7)	0.0096 (10)	0.0034 (3)	0.0035 (4)

The calculated efficiencies for the $LaBr_3(Ce)$ detector were larger than those calculated for the NaI(Tl) detector over the entire energy range. This behavior can be understood by comparing the densities of both crystals, which are 3.67 g/cm^3 for the NaI(Tl) and 5.08 g/cm^3 for the $LaBr_3(Ce)$.

The efficiency curves represented in Fig. 5 do not account for the filter retention efficiency, which in practice is assumed to be 100%. It is important to remark that only particulate forms of the isotopes are captured in the filter. Thus, the real activity concentrations in air could be underestimated. In particular, iodine isotopes are of interest, and hence, some hypothesis about the percentage of particulates of iodine should be accounted to provide more realistic values of their concentration of activity in air.

C. Measurement Capabilities

To study the measurement capabilities of each of the developed RARM-Fs, some values of the MDACs for the ^{137}Cs are reported in Table I. These values, which can vary depending on the natural background, are provided to have an estimation of the RARM-F capabilities. However, it is not possible to compare them directly because the monitors are slightly different. In fact, the $LaBr_3(Ce)$ includes some improvements in comparison with the NaI(Tl) one that have made it possible to obtain higher flows without breaking the filter. Thus, the average flows were 4.1 m^3/h and 10.4 m^3/h for the NaI(Tl) and $LaBr_3(Ce)$ monitors, respectively. Further work is being carried out to increase the flows even more, which will make it possible to obtain lower MDACs.

For comparison, for a 10 min measurement, the MDAC obtained with direct measurement with a 1.5" x 1.5" $LaBr_3$ for the ^{137}Cs is 30 Bq/m^3 [3], which is much larger than those obtained with RARM-F. Besides, these differences would be even larger if the performances would be compared at larger integration times.

Finally, the results in Table I show that the measurement capabilities of the RARM-F for ^{137}Cs are more dependent on the background when the NaI(Tl) detector is used. This is a consequence of the low resolution of this detector, which cannot clearly resolve the peak from ^{214}Bi at 609 keV from the one of ^{137}Cs at 662 keV, producing an overlap between them. This effect is no longer produced in the $LaBr_3(Ce)$ detector, where the variation on the MDAC values depends basically on the variation of the background due to Compton scattering of higher energy photons.

V. Conclusions

A Real-time Airborne Radioactivity Monitor using gamma-ray spectrometry on a particulate Filter (RARM-F) was developed. The monitor can be operated with either a NaI(Tl) detector or a $\mathrm{LaBr_3(Ce)}$ detector.

To achieve optimal performance, the RARM-F was fully calibrated (energy, resolution and efficiency calibrations) using experimental data and Monte Carlo simulations with the EGS5 code system.

The performance of the different RARM-Fs with different crystals was evaluated with some values of the MDACs for $^{137}\mathrm{Cs}$. The results show better performance for these monitors in comparison with other measuring directly in the environment.

Finally, the RARM-F is ready to be used in an automatic real-time environmental radiation surveillance network by allowing the isotope identification and quantifications, and thus, the establishment of automatic alerts based on the limits provided by legislation.

Acknowledgment

Part of this research was performed using the resources of the CESCA (Centre de Supercomputació de Catalunya).

References

[1] R. Casanovas, J. J. Morant, M. López, I. Hernández-Girón, E. Batalla, and M. Salvadó, "Performance of data acceptance criteria over 50 months from an automatic real-time environmental radiation surveillance network," *J. Environ. Radioact.*, vol. 102, pp. 742–748, 2011.

[2] S. M. Bowyer, H. S. Miley, R. C. Thompson, and C. W. Hubbard, "Automated particulate sampler for comprehensive test ban treaty verification (the DOE radionuclide aerosol sampler/analyzer," *IEEE Trans. Nucl. Sci.*, vol. 44, no. 3, pp. 551–556, Jun. 1997.

[3] A. Mattila, H. Toivonen, K. Vesterbacka, M. Leppänen, S. Salmelin, and A. Pelikan, "Radiation monitoring network with spectrometric capabilities: Implementation of $\mathrm{LaBr_3}$ spectrometers to the Finnish network," in *Proc. 3rd Eur. IRPA Congr.*, Helsinki, Finland, 2010, pp. 1958–1966 [Online]. Available: http://www.irpa2010europe.com/pdfs/proceedings/S12-P12.pdf.

[4] J. B. Forrester, F. F. Carty, L. Comes, J. C. Hayes, H. S. Miley, S. J. Morris, M. Ripplinger, R. W. Slaugh, and P. Van Davelaar, "Engineering upgrades to the radionuclide aerosol sampler/analyzer for the CTBT international monitoring system," *J. Radioanal. Nucl. Chem.*, vol. 296, pp. 1055–1060, 2013.

[5] R. Casanovas, M. Salvadó, M. Lopez, C. Tapia, and A. de Blas, "Estación de identificación y medida en tiempo real de la radiactividad ambiental gamma mediante espectrometría sobre filtro de papel (in Spanish)," ES Patent Application P201230408, Mar. 16, 2012 [Online]. Available: http://www.oepm.es/pdf/ES/0000/000/02/42/58/ES-2425801_A1.pdf.

[6] R. Casanovas, J. J. Morant, and M. Salvadó, "Energy and resolution calibration of NaI(Tl) and $\mathrm{LaBr_3(Ce)}$ scintillators and validation of an EGS5 Monte Carlo user code for efficiency calculations," *Nucl. Intrum. Methods Phys. Res. A*, vol. 675, pp. 78–83, 2012.

[7] R. Casanovas, J. J. Morant, and M. Salvadó, "Temperature peak-shift correction methods for NaI(Tl) and $\mathrm{LaBr_3(Ce)}$ gamma-ray spectrum stabilization," *Radiat. Meas.*, vol. 47, pp. 588–595, 2012.

[8] L. A. Currie, "Limits for qualitative detection and quantitative determination," *Anal. Chem.*, vol. 40, pp. 586–593, 1968.

[9] H. Hirayama, Y. Namito, A. F. Bielajew, S. J. Wilderman, and W. R. Nelson, The EGS5 Code System Stanford, CA, USA, Rep. SLAC-R-730, Dec. 19, 2005 [Online]. Available: http://slac.stanford.edu/cgi-wrap/getdoc/slac-r-730.pdf.

[10] M. J. Berger, J. S. Coursey, M. A. Zucker, and J. Chang, ESTAR, PSTAR, and ASTAR: Computer Programs for Calculating Stopping-Power and Range Tables for Electrons, Protons, and Helium Ions (version 1.2.3) [Online]. Available: http://physics.nist.gov/Star